Orbital interactions and charge redistribution in weak hydrogen bonds: The Watson–Crick AT mimic adenine-2,4-difluorotoluene

Célia Fonseca Guerra and F. Matthias Bickelhaupt[a)]
Afdeling Theoretische Chemie, Scheikundig Laboratorium der Vrije Universiteit, De Boelelaan 1083, NL-1081 HV Amsterdam, The Netherlands

(Received 29 April 2003; accepted 27 May 2003)

The discovery by Kool and co-workers that 2,4-difluorotoluene (F) mimics thymine (T) in DNA replication has led to a controversy about the question if this mimic has the capability of forming hydrogen bonds with adenine (A). In the present study, we address not only the question about the *strengths* of the hydrogen bonds in AF as compared to those in AT but we focus in particular on the *nature* of these interactions. Thus, we have analyzed AF and AT at the BP86/TZ2P level of density functional theory (DFT). In line with previous experience, this approach is shown to achieve close agreement with the available data from *ab initio* computations and experiment: the complexation energy of AF (−3.2 kcal/mol) is confirmed to be much weaker indeed than that of AT (−13.0 kcal/mol). Interestingly, the weak hydrogen bonds in AF still possess a significant orbital interaction component that resembles the situation for the more strongly bound AT, as follows from (1) an analysis of the orbital electronic structure of AF and AT, (2) a quantitative decomposition of the A–F and A–T bond energies, as well as (3) a quantitative decomposition of the charge redistribution associated with the A–F and A–T interactions based on the Voronoi deformation density (VDD) method. The VDD method has been further developed such that the charge redistribution ΔQ per atom can be decomposed into a component associated with the Pauli repulsive orbital interactions and a component associated with the bonding orbital interactions: $\Delta Q = \Delta Q_{\mathrm{Pauli}} + \Delta Q_{\mathrm{oi}}$. Implications of our findings for the mechanism of DNA replication are discussed. © *2003 American Institute of Physics.* [DOI: 10.1063/1.1592494]

I. INTRODUCTION

DNA replication is at the core of life and an increasing number of studies aims at unraveling the mechanism of this complex biochemical reaction that, in spite of much effort, is still incompletely understood.[1–3] In the standard model, the immensely high accuracy with which this process occurs is ascribed to the specificity of the hydrogen bonds in the Watson–Crick pairs adenine–thymine (AT) and guanine–cytosine (GC).[1] This view has recently been challenged by experiments with artificial nucleotides [2,3(a)–3(g)] or with alterations of the binding pocket of polymerase,[3(h)–3(j)] which show that geometric constraints are important for the replication fidelity. Experiments[3(n)–3(s)] with hydrophobic base pairs suggest that hydrophobicity may also be a sufficient driving force for selective replication. In this paper we focus on the results by Kool and co-workers.[2] They proposed that *not* Watson–Crick hydrogen bonding but steric effects, that is, the shape of DNA bases is mainly responsible for the high fidelity of DNA replication. This idea evolved from a series of elegant experiments in which they showed, amongst others, that 2,4-difluorotoluene (F), an isoster of thymine (T), encodes in a template strand the DNA polymerase-catalyzed insertion of deoxyadenosine triphosphate (dATP) and that adenine (A) encodes the insertion of the deoxynucleoside triphosphate of difluorotoluene (dFTP), in spite of the supposed apolarity and absence of hydrogen bonding ability of F (see Chart 1).[2(f)–2(h)] On the other hand, they suggested that hydrogen bonding may still play an important role in the proofreading mechanism.[2(m)]

The introduction of the steric model has led to a contro-

Chart 1

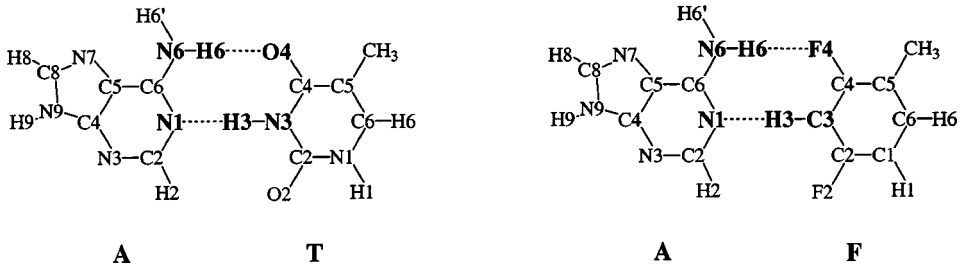

a)Electronic mail: bickel@chem.vu.nl

versy in which experimental[2–5] and theoretical[6–8] arguments are raised both against and in favor of the standard model. Recently, we have proposed an alternative model[8] for the replication of DNA in which both factors, steric shape as well as hydrogen bonding interactions, play a key role *simultaneously*. In our model, the event of molecular recognition, that is, the occurrence of a low barrier for the insertion reaction of a deoxynucleoside triphosphate into a primer-template complex is promoted in two complementary ways: (1) the shape of the bases must be such that they can adopt the Watson–Crick geometry without (too much) steric repulsion; (2) the barrier can be further reduced if there is in addition a stabilizing interaction between the bases in the base pair. We stress at this point that the entire chemical process of nucleotide insertion is a complex multistep reaction in which also other factors contribute to the overall barrier height,[2,3] such as solvation, hydrophobicity, stacking, conformational changes in the primer–template–polymerase complex as well as the $S_N2@P$ substitution reaction that eventually leads to the elongation of the back bone in the primer DNA strand.

In the present study, we focus on the event of molecular recognition between the template and the incoming DNA base in the active site of polymerase. In particular, we wish to address the question if F, in spite of the N–H and C═O groups of T having been replaced by C–H and C–F (Chart 1), can still form hydrogen bonds with A that are strong enough (see, for example, Refs. 9–11) to play a role of importance in the selective enzyme-catalyzed molecular recognition between A and F. It is known that the A–F bonding energy is only one third of the A–T bonding energy.[6,8] We will argue, however, that the net bond strength is insufficient for characterizing a hydrogen bond and that understanding and predicting the role and behavior of the hydrogen bonds in AF during DNA replication requires knowledge of the different components of the bonding mechanism.

Thus, we have conducted a detailed density functional theory (DFT) study of the hydrogen bonding mechanism in AF as compared to that in AT. This is done at the BP86/TZ2P level of the generalized gradient approximation (GGA), which has been shown previously to adequately describe hydrogen bonds in Watson–Crick pairs as well as mismatched pairs of DNA bases but also in the more weakly bound water dimer.[12] Based on the conceptual framework provided by Kohn–Sham molecular orbital (KS–MO) theory,[13] we have investigated the hydrogen bonding mechanism through an analysis of the orbital electronic structure and a quantitative decomposition of the A–F and A–T bond energies into the electrostatic attraction, the repulsive orbital interactions (Pauli repulsion) and the bonding orbital interactions. In particular, we wish to find out if covalent bonding (i.e., charge-transfer or donor–acceptor orbital interactions) that was found previously to occur in the more firmly bound natural Watson–Crick base pairs[14] also contributes significantly to the stability of the weak hydrogen bonds of AF or if the latter are a purely electrostatic phenomenon.

Complementary to the electronic structure and bond energy analyses, we have carried out a quantitative decomposition of the charge redistribution associated with the A–F and A–T interactions based on the Voronoi deformation density (VDD) method.[14,15] For this purpose, the VDD method has been further developed such that the charge redistribution ΔQ per atom can be decomposed into a component associated with the Pauli repulsion and a component associated with the bonding orbital interactions: $\Delta Q = \Delta Q_{\text{Pauli}} + \Delta Q_{\text{oi}}$. Full details of our analyses and the new developments of the VDD method are reported, and we discuss the implications of our findings for the mechanism of DNA replication.

II. THEORETICAL METHODS

A. General procedure

All calculations were performed using the Amsterdam Density Functional (ADF) program.[16] The numerical integration was performed using the procedure developed by te Velde *et al.*[16(g),16(h)] The MOs were expanded in a large uncontracted set of Slater-type orbitals (STOs) containing diffuse functions: TZ2P (no Gaussian functions are involved).[16(i)] The basis set is of triple-ζ quality for all atoms and has been augmented with two sets of polarization functions, i.e., $3d$ and $4f$ on C, N, O, F, and $2p$ and $3d$ on H. The $1s$ core shell of carbon, nitrogen, oxygen, and fluorine were treated by the frozen-core approximation.[16(c)] An auxiliary set of *s, p, d, f,* and *g* STOs was used to fit the molecular density and to represent the Coulomb and exchange–correlation potentials accurately in each self-consistent-field cycle.[16(j)] Geometries (optimized through analytical gradient techniques)[16(k)] and energies were calculated using the generalized gradient approximation (GGA): exchange is described by Slater's $X\alpha$ potential[16(l)] with corrections due to Becke[16(m),16(n)] added self-consistently and correlation is treated in the Vosko–Wilk–Nusair (VWN) parametrization[16(o)] with nonlocal corrections due to Perdew[16(p)] added, again, self-consistently (BP86).[16(q)]

B. Bond energy decomposition

The overall bond energy ΔE is made up of two major components [Eq. (1)],

$$\Delta E = \Delta E_{\text{prep}} + \Delta E_{\text{int}}. \tag{1}$$

In this formula, the preparation energy ΔE_{prep} is the amount of energy required to deform the separate bases from their equilibrium structure to the geometry that they acquire in the pair. The interaction energy ΔE_{int} corresponds to the actual energy change when the prepared bases are combined to form the base pair. It is analyzed for the hydrogen-bonded model systems in the framework of the Kohn–Sham MO model using a Morokuma-type decomposition[17] of the bond energy into electrostatic interaction, exchange repulsion (or Pauli repulsion), and (attractive) orbital interactions [Eq. (2)],[13]

$$\Delta E_{\text{int}} = \Delta V_{\text{elst}} + \Delta E_{\text{Pauli}} + \Delta E_{\text{oi}}. \tag{2}$$

The term ΔV_{elst} corresponds to the classical electrostatic interaction between the unperturbed charge distributions of the prepared (i.e., deformed) bases and is usually attractive. The Pauli-repulsion ΔE_{Pauli} comprises the destabilizing interactions between occupied orbitals and is responsible for the

steric repulsion. The orbital interaction ΔE_{oi} in any MO model, and therefore also in Kohn–Sham theory, accounts for charge transfer (i.e., donor–acceptor interactions between occupied orbitals on one moiety with unoccupied orbitals of the other, including the HOMO–LUMO interactions) and polarization (empty/occupied orbital mixing on one fragment due to the presence of another fragment). Since the Kohn–Sham MO method of DFT in principle yields exact energies and, in practice, with the available density functionals for exchange and correlation, rather accurate energies, we have the special situation that a seemingly one-particle model (an MO method) in principle completely accounts for the bonding energy. In particular, the orbital-interaction term of the Kohn–Sham theory comprises the often distinguished attractive contributions charge transfer, induction (polarization), and dispersion. One could in the Kohn–Sham MO method try to separate polarization and charge transfer, as has been done by Morokuma in the Hartree–Fock model, but this distinction is not sharp. In fact, contributions such as induction and charge transfer, and also dispersion, can be given an intuitive meaning, but whether, or with what precision, they can be quantified, remains a controversial subject. In view of the conceptual difficulties we refrain from further decomposing the KS orbital interaction term, except by symmetry, see below. We have observed that the orbital interactions are mostly of the donor–acceptor type (e.g., an N or O lone pair on one moiety with N–H σ^* orbital of the other), and we feel it is therefore justified to denote the full orbital interaction term for brevity just as ''charge transfer'' or ''covalent'' contribution, as opposed to the electrostatic and Pauli repulsion contributions. However, the straightforward denotation ''orbital interaction'' avoids confusion with the charge-transfer energy, which features in other elaborate decomposition schemes[18] that also give rise to induction and dispersion contributions, which we do not attempt to quantify but which are all lumped together in the Kohn–Sham orbital interaction.

The orbital interaction energy can be decomposed into the contributions from each irreducible representation Γ of the interacting system [Eq. (3)] using the extended transition state (ETS) scheme developed by Ziegler and Rauk.[17(c)–17(e)] In systems with a clear σ, π or A', A'' separation (such as our AF and AT base pairs), this symmetry partitioning proves to be most informative,

$$\Delta E_{oi} = \sum_{\Gamma} \Delta E_{\Gamma}. \tag{3}$$

C. Analysis of the charge distribution

The electron density distribution is analyzed using the Voronoi deformation density (VDD) method introduced in Ref. 15. The VDD charge Q_A is computed as the (numerical) integral of the deformation density $\Delta\rho(\mathbf{r}) = \rho(\mathbf{r}) - \Sigma_B \rho_B(\mathbf{r})$ associated with the formation of the molecule from its atoms in the volume of the Voronoi cell of atom A [Eq. (4)]. The Voronoi cell of atom A[16(h),19] is defined as the compartment of space bounded by the bond midplanes on and perpendicular to all bond axes between nucleus A and its neighboring nuclei (cf. the Wigner–Seitz cells in crystals),

$$Q_A = -\int_{\text{Voronoi cell A}} \left(\rho(\mathbf{r}) - \sum_B \rho_B(\mathbf{r}) \right) d\mathbf{r}. \tag{4}$$

Here, $\rho(\mathbf{r})$ is the electron density of the molecule and $\Sigma_B \rho_B(\mathbf{r})$ the superposition of atomic densities ρ_B of a fictitious promolecule without chemical interactions that is associated with the situation in which all atoms are neutral. The interpretation of the VDD charge Q_A is rather straightforward and transparent. Instead of measuring the amount of charge associated with a particular atom A, Q_A directly monitors how much charge flows, due to chemical interactions, out of ($Q_A > 0$) or into ($Q_A < 0$) the Voronoi cell of atom A, that is, the region of space that is closer to nucleus A than to any other nucleus.

The chemical bond between two molecular fragments can be analyzed by examining how the VDD atomic charges of the fragments change due to the chemical interactions. In Ref. 14, however, we have shown that Eq. (4) leads to small artifacts that prohibit an accurate description of the subtle changes in atomic charges that occur in case of weak chemical interactions, such as hydrogen bonds. This is due to the so-called front-atom problem that, in fact, all atomic-charge methods suffer from. To resolve this problem and, thus, enabling a correct treatment of even subtle changes in the electron density, the change in VDD atomic charges ΔQ_A is defined by Eq. (5), which relates this quantity directly to the deformation density $\rho_{pair}(\mathbf{r}) - \rho_{base1}(\mathbf{r}) - \rho_{base2}(\mathbf{r})$ associated with forming the overall molecule (i.e., the base pair) from the joining molecular fragments (i.e., base1 and base2),[14]

$$\Delta Q_A = -\int_{\substack{\text{Voronoi cell A} \\ \text{in pair}}} [\rho_{pair}(\mathbf{r}) - \rho_{base1}(\mathbf{r}) - \rho_{base2}(\mathbf{r})] d\mathbf{r}. \tag{5}$$

Again, ΔQ_A has a simple and transparent interpretation: it directly monitors how much charge flows out of ($\Delta Q_A > 0$) or into ($\Delta Q_A < 0$) the Voronoi cell of atom A as a result of the chemical interactions between base1 and base2 in the base pair.

Furthermore, ΔQ_A can also be decomposed into ΔQ_A^{σ} and ΔQ_A^{π}, the contributions of the σ- and π-deformation densities, respectively [Eq. (6)],

$$\Delta Q_A^{\Gamma} = -\int_{\substack{\text{Voronoi cell A} \\ \text{in pair}}} [\rho_{pair}^{\Gamma}(\mathbf{r}) - \rho_{base1}^{\Gamma}(\mathbf{r}) - \rho_{base2}^{\Gamma}(\mathbf{r})] d\mathbf{r}. \tag{6}$$

Here, the density ρ^{Γ} is obtained as the sum of orbital densities of the occupied molecular orbitals belonging to the irreducible representation Γ [Eq. (7)],

$$\rho^{\Gamma} = \sum_{i \in \Gamma}^{\text{occ}} |\psi_i^{\Gamma}|^2. \tag{7}$$

Later on, in Sec. III C, we show how ΔQ_A^{σ} and ΔQ_A^{π} can be further partitioned into contributions caused by Pauli repulsion and bonding orbital interactions, respectively, thus constituting a complete bond analysis tool that complements the energy decomposition scheme presented above in Sec. II B.

TABLE I. Analysis of the base-pairing interaction of adenine (A) with thymine (T), 2,4-difluorotoluene (F), and toluene (B).[a]

	AT	AF	AF*[b]	AB*[b]
Hydrogen bond distances (in Å)				
N6–X4[c]	2.85	3.23	2.85	2.85
N1–Y3[d]	2.81	3.39	2.81	2.81
Bond energy decomposition (in kcal/mol)				
ΔE_{Pauli}	38.7	7.8	41.5	36.7
ΔV_{elstat}	−31.8	−7.0	−22.6	−15.5
$\Delta E_{\text{Pauli}}+\Delta V_{\text{elstat}}$	6.9	0.8	18.9	21.2
ΔE_{σ}	−20.4	−3.8	−15.0	−11.4
ΔE_{π}	−1.7	−0.2	−1.0	−0.6
ΔE_{oi}	−22.1	−4.0	−16.0	−12.0
ΔE_{int}	−15.2	−3.2	2.9	9.2
ΔE_{prep}	2.2	0.2		
ΔE	−13.0	−3.0		
ΔE (C_1)	−13.0	−3.0		

[a]BP86/TZ2P.
[b]In AF* and AB*, hydrogen bonds have been compressed to the equilibrium distances of AT.
[c]X4 = O4, F4, and H4 in the bases T, F, and B.
[d]Y3 = N3, C3, and C3 in the bases T, F, and B.

III. RESULTS AND DISCUSSION

A. Geometries and hydrogen bond strengths

The results of our BP86/TZ2P study on the AF and AT complexes are summarized in Table I (energies) and Fig. 1 (geometries). We have shown previously that the BP86/TZ2P approach leads to excellent agreement with experiment and traditional *ab initio* computations for Watson–Crick AT and GC base pairs, for mismatched DNA base pairs and for the weakly bound water dimer.[12] In the present study, we have optimized AF both in C_s symmetry and without any geometry restrictions in C_1 symmetry. Both approaches yield, within our numerical precision, the same geometries and bond energies. For the bond analyses, we use the former geometries because the decomposition of the orbital interactions into contributions of the σ and π electrons (i.e., A′ and A″) requires exactly C_s-symmetric base pairs.

The base-pairing energy ΔE (at 0 K) for AF amounts to −3.0 kcal/mol at BP86/TZ2P and is thus approximately four-times weaker than the corresponding value of −13.0 kcal/mol for AT (Table I).[12(a),12(b)] The N6–F4 and N1–C3 hydrogen bond distances of 3.23 and 3.39 Å in AF substantially exceed the corresponding N6–O4 and N1–N3 distances of 2.85 and 2.81 Å in AT (Table I). The base-pairing interaction in AF has no noticeable effect on the adenine N6–H6 and 2,4-difluorotoluene C3–H3 bond lengths [see Fig. 1; for adenine, see Ref. 12(a)], at variance with the situation for AT where the corresponding bonds elongate by 0.02–0.05 Å due to the stronger charge–transfer interactions in the latter base pair.[14]

The above BP86/TZ2P results agree well with the available data from literature that AF is rather weakly bound, by 3–4 kcal/mol, with hydrogen bond distances of 3.2–3.4 Å. Experimental data have, to our knowledge, not been reported. Our AF base-pairing energy of −3.0 kcal/mol agrees best with the B3LYP/6-31G(d,p) value of −3.2 kcal/mol obtained by Meyer and Sühnel.[6(g)] Base-pairing energies at MP2 are about 1 kcal/mol more stabilizing: −4.18 kcal/mol at MP2/6-31G*(0.25)//HF/6-31G**[6(c)] and −3.8 kcal/mol at the MP2/6-31G(d,p)//HF/6-31G(d,p).[6(g)] Our N6–F4

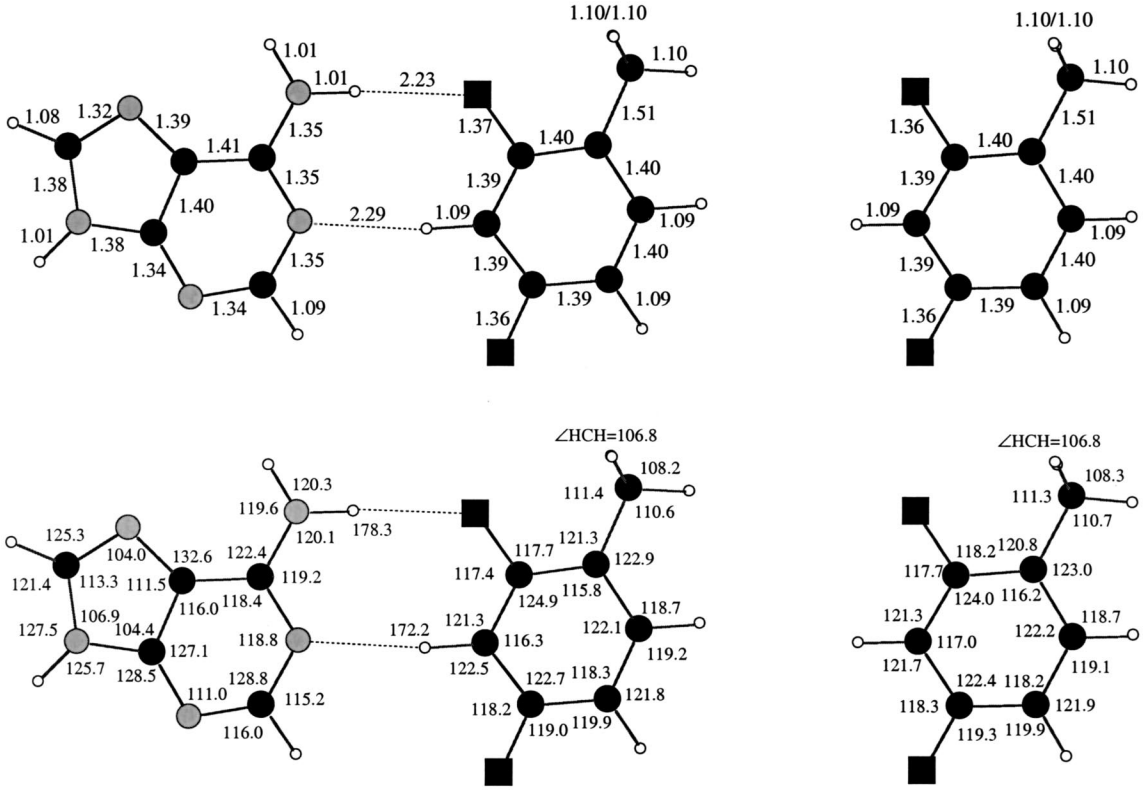

FIG. 1. Geometry of AF and F (in Å, degrees) from unconstrained optimizations at BP86/TZ2P (see Chart 1).

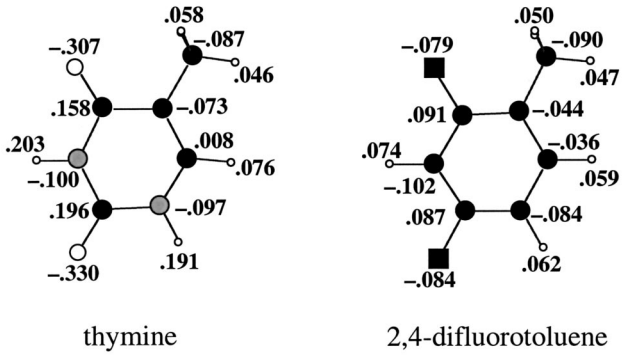

FIG. 2. VDD atomic charges (in e) of thymine and 2,4-difluorotoluene obtained at BP86/TZ2P (see Chart 1).

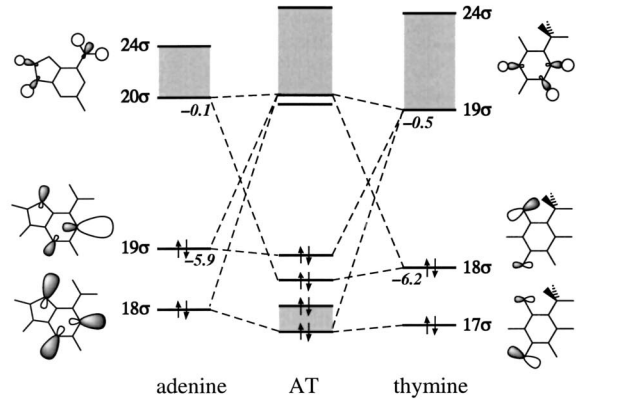

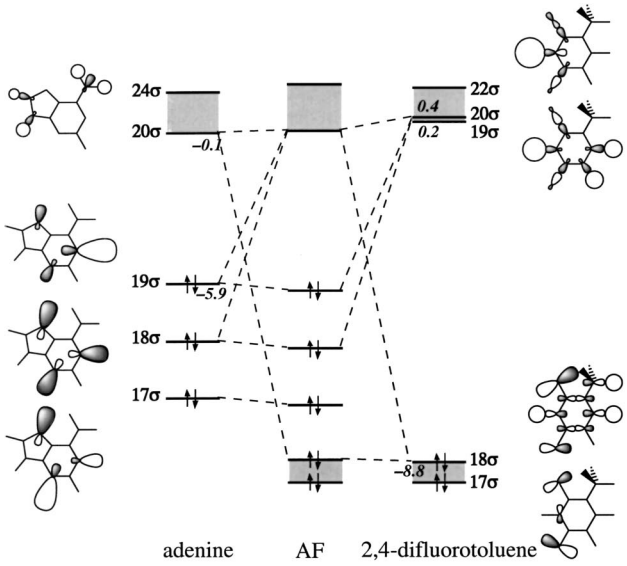

FIG. 3. Frontier orbital interactions (in the σ-electron system) between adenine and thymine in AT and between adenine and 2,4-difluorotoluene in AF from Kohn–Sham DFT analyses at BP86/TZ2P, with σ_{HOMO} and σ_{LUMO} energies of the bases (in eV). The group of lowest unoccupied orbitals involved is represented as a gray block. Selected orbitals of adenine (17σ to 20σ), thymine (17σ to 19σ) and difluorotoluene (17σ, 18σ, 20σ, 22σ) are schematically represented.

and N1–C3 hydrogen bond distances of 3.23 and 3.39 Å are similar in magnitude to the B3LYP/6-31G(d,p) values of 3.44 and 3.10Å.[6(g)] Note, however, that BP86/TZ2P yields the N6–F4 bond shorter than the N1–C3 bond while it is the other way around at B3LYP/6-31G(d,p). This is in line with the extremely shallow potential energy surface (PES) that we find for the hydrogen bonds in AF. This makes that subtle changes in the computational model cause larger changes in the soft geometry parameters without much consequences for the bond energy ΔE.

B. Nature of the hydrogen bond in AF

1. F versus T electronic structure

First, we examine the bonding capability of 2,4-difluorotoluene (F) and how this differs from thymine (T) through an analysis of the electronic structure. Previously, we have shown how the electronic complementarity of the DNA bases in the Watson–Crick base pairs AT and GC yields the formation of stable hydrogen bonds in two ways: (i) positively charged H atoms in front of negatively charged N or O atoms lead to a favorable electrostatic attraction; (ii) lone pairs on N and O of one base directed toward and overlapping with unoccupied N–H σ^* orbitals of the other base lead to an important additional stabilization through donor–acceptor orbital interactions (see Fig. 3, top). In both respects, the electronic structure of F differs to some extent from that of T.

In the first place, F is less polar than T. The dipole moment of T amounts to 4.33 D (4.24 D for the deformed base in the geometry of the AT pair) and is thus more than twice as large as that of F, which is only 1.85 D (1.88 D for the deformed base in the geometry of the AF pair). Note however that, in the complex, the bases are too close to each other to be treated as point dipoles. A more realistic picture emerges if one considers the local charge distribution in more detail. This is done in Fig. 2, which shows the VDD atomic charges [Eq. (5)][15] of the separate, noninteracting bases T and F (see Chart 1 for atom numbering). It appears that qualitatively F has the same charge distribution as T: hydrogen bond-acceptor atoms are negatively charged while the corresponding hydrogen atoms carry a positive charge. However, the magnitude of these atomic charges is much smaller in F than in T. The atomic charge of F4 in F is -0.079e, which has to be compared with -0.307e of O4 in T. Furthermore, H3 has an atomic charge of $+0.074$e in F and $+0.203$e in T. As a consequence, the electrostatic attraction between A and F is smaller than between A and T (*vide infra*).

The orbital electronic structure reveals that, compared to T, F is a poor electron donor and a poor electron acceptor, as can be seen in Fig. 3. The occupied orbital with lone pair-character on the F4 atom in F (i.e., the 18σ MO at -8.8 eV) is much lower in energy than the corresponding orbital with lone pair-character on the O4 atom in T (i.e., the 18σ MO at -6.2 eV). Also, the unoccupied orbitals with sizeable C3–H3 σ^* character in F (i.e., the 20σ MO at 0.4 eV and virtuals at higher energy) are somewhat higher in energy than the corresponding N3–H3 σ^* orbitals in T (i.e., the 19σ MO at -0.5 eV and virtuals at higher energy). The unoccupied 19σ MO of F, at 0.2 eV, has no significant C3–H3 σ^* character and can, therefore, not act as an acceptor orbital (even

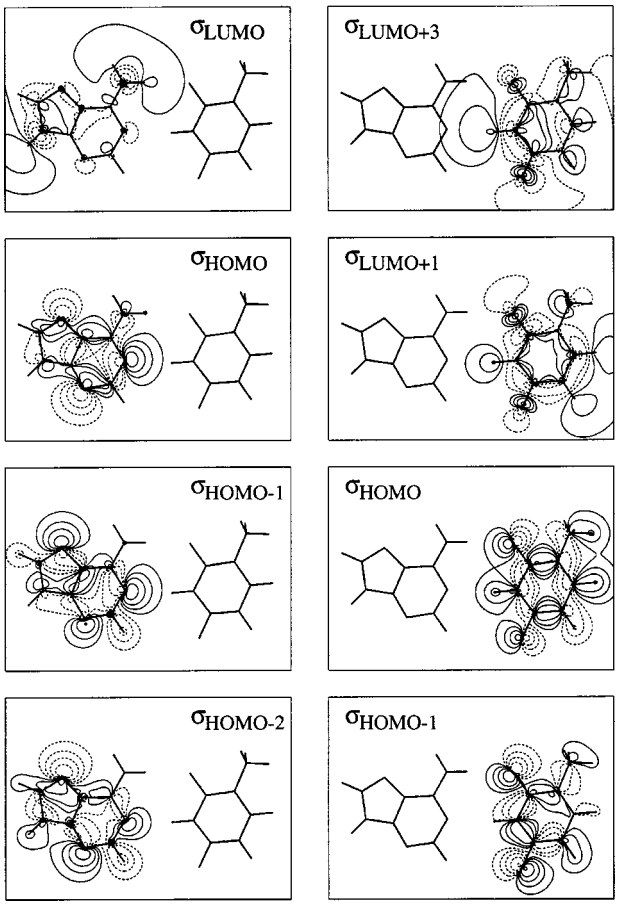

FIG. 4. Contour plots of selected orbitals of adenine (left panel) and 2,4-difluorotoluene (right panel) computed at BP86/TZ2P (scan values: ± 0.5, ± 0.2, ± 0.1, ± 0.05, ± 0.02; solid and dashed contours refer to positive and negative values, respectively). For each orbital, both its own base and the other base in the AF pair are shown as wire frames.

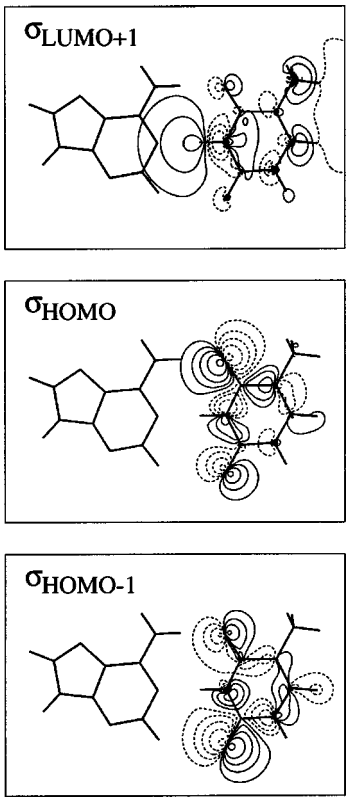

FIG. 5. Contour plots of selected orbitals of thymine computed at BP86/TZ2P (see also legend to Fig. 4). For each orbital, both its own base (thymine) and the other base (adenine) in the AT pair are shown as wire frames.

though it is at lower orbital energy than the 20σ at 0.4 eV) in the hydrogen bond with a lone pair on the N1 atom in A. The low-energy lone pair and high-energy σ^* orbitals of F cause the A–F donor–acceptor orbital interactions to be less stabilizing than the corresponding A–T orbital interactions (*vide infra*).

The shapes of DNA-base orbitals are displayed only schematically in Fig. 3, which focuses on their main characteristics. A more realistic representation is provided by the contour plots of Figures 4(A), 4(F), and 5(T). None of the orbitals is localized entirely on one N or O atom or N–H bond, of course, but still one can clearly distinguish the lone-pair and σ^* orbitals of the front atoms, i.e., the N, O, and N–H groups that are involved in hydrogen bonds with the other base. The $\sigma_{\text{HOMO-1}}$ and σ_{HOMO} orbitals of adenine (18σ and 19σ in Fig. 3), for example, have pronounced lone-pair character on the N1 atom, and the σ_{LUMO} of adenine (20σ in Fig. 3) has a definite N6–H6 σ^* feature. Likewise, we can recognize the lone-pair and σ^* orbitals in, respectively, 2,4-difluorotoluene (Fig. 4) and thymine (Fig. 5). Note, however, that the orbitals that correspond with each other in F and T, respectively, differ strikingly with regard to their precise shape and the extent to which lone-pair or σ^* character on a particular atom or bond dominates (in terms of amplitude) over other features of the orbital. The σ_{HOMO} of T (18σ in Fig. 3, top), for example, behaves in the A–T orbital interactions as the lone pair on O4 (*vide infra*) because it has significantly more amplitude on that oxygen atom than on O2 (Fig. 5). The σ_{HOMO} of F (18σ in Fig. 3, bottom), on the other hand, has approximately the same amount of lone-pair character on F4 and F2 and, more importantly, it has a sizeable amplitude on H3 that stems from pronounced C3–H3 σ bonding character (Fig. 4). This is due to the fact that the $2s$ and $2p$ AOs of the fluorine atom are lower in energy than those of oxygen and therefore they interact and mix more strongly with the σ bonding orbitals of a C–H (or N–H) bond. Likewise, the $\sigma_{\text{LUMO+1}}$ of T (20σ contained in the gray block in Fig. 3, top) is strongly N3–H3 σ^* antibonding with a large lobe on H3 but it has no important feature on the C4–O4 bond (Fig. 5). At variance, the $\sigma_{\text{LUMO+1}}$ of F (20σ contained in the gray block in Fig. 3, bottom) has, in addition to its C3–H3 σ^* antibonding character, a striking C4–F4 σ^* feature (Fig. 4). The consequences of the orbitals on F being more delocalized over the base than the orbitals of T is discussed later on, in Sec. III D.

2. A–F versus A–T hydrogen bonding mechanism

The quantitative hydrogen-bond energy decomposition reveals that AF has both weaker electrostatic attraction ΔV_{elstat} and weaker orbital interactions ΔE_{oi} than AT (see Table I). The values of ΔV_{elstat} and ΔE_{oi} are only -7.0 and -4.0 kcal/mol for AF while they amount to -31.8 and -22.1 kcal/mol for AT. This is in good agreement with the

TABLE II. Overlaps between σ frontier orbitals of the bases in AF.[a]

$\langle\sigma_A\|\sigma_F\rangle$	$\|17\sigma_F\rangle$	$\|18\sigma_F\rangle$	$\|20\sigma_F\rangle$	$\|22\sigma_F\rangle$
$\langle 17\sigma_A\|$	0.001	0.008	0.013	0.043
$\langle 18\sigma_A\|$	0.001	0.028	0.040	0.151
$\langle 19\sigma_A\|$	0.001	0.033	0.040	0.168
$\langle 20\sigma_A\|$	0.007	0.044	0.074	0.172
$\langle 21\sigma_A\|$	0.009	0.054	0.105	0.191
$\langle 22\sigma_A\|$	0.004	0.046	0.023	0.088
$\langle 23\sigma_A\|$	0.014	0.063	0.003	0.130
$\langle 24\sigma_A\|$	0.023	0.047	0.101	0.114

[a]BP86/TZ2P.

mimic F being less polar (Fig. 2) and having poor electron donor and acceptor capabilities compared to T (Fig. 3). Note that *all* energy terms of AF are small, not only ΔV_{elstat} and ΔE_{oi} but also the Pauli repulsive orbital interactions between occupied orbitals on A and F. The reason is that the reduced bonding capability of F compared to T causes an expansion of the equilibrium hydrogen bond distances (from 2.85 and 2.81 Å in AT to 3.23 and 3.39 Å in AF). This, in turn, leads to a further reduction of ΔV_{elstat} and ΔE_{oi} and it also causes a weakening of ΔE_{Pauli}, which would otherwise be similar for AF and AT (*vide infra*).

The orbital interactions ΔE_{oi} play a nearly as important role in AF as they do in AT, providing 36% of all bonding forces ($\Delta V_{\text{elstat}}+\Delta E_{\text{oi}}$) in the former and 41% in the latter complex. Without the bonding orbital interactions, the net interaction energy of AT and AF in their equilibrium geometries would even be repulsive by 6.9 and 0.8 kcal/mol (see $\Delta E_{\text{Pauli}}+\Delta V_{\text{elstat}}$ in Table I). This is in line with our results on Watson–Crick and mismatched pairs of DNA bases,[12(b),12(c),14] and it provides further evidence against the common idea[8,20] that weak hydrogen bonds involving a fluorine atom as proton acceptor or a C–H group as proton donor are mainly electrostatic phenomena.

The A–F and A–T orbital interaction diagrams in Fig. 3 emerge from our Kohn–Sham MO analyses and show schematically the main mixing pattern of the fragment orbitals in the σ-electron systems of the respective base pairs. The overlaps between the fragment orbitals in AF are collected in Table II (for AT, see Ref. 14). The orbital interactions in the two base pairs have in common that they are provided by donor–acceptor interactions from lone-pair orbitals on A to σ^* orbitals on F or T through the N1···H3–Y3 hydrogen bond (Y3=C3 or N3) and *vice versa* from lone-pair orbitals on F or T to σ^* orbitals on A through the N6–H6···X4 hydrogen bond (X4=F4 or O4). The main difference is a weaker mixing due to the much lower energy of the F4 lone-pair orbitals of 2,4-difluorotoluene (F) as compared to the O4 lone-pair orbitals of thymine (T). Furthermore, the unoccupied 19σ MO of F does, in contrast to the 19σ of T, not act as an acceptor orbital for the lone pair on the N1 atom in A because it has no significant C3–H3 σ^* character (*vide supra*). Additional support for the donor–acceptor (or charge-transfer) character of the bonding orbital interactions comes from the VDD charge decomposition analysis in Sec. III D.

3. A–F versus A–T interaction in DNA polymerase's active site

The above results demonstrate that percentage wise orbital interactions are still important in the A–F hydrogen bonds. Two important questions remain, however. First, is F really (as proposed in Kool's steric model[2]) an isoster of T if it leads to such an enormous elongation of hydrogen bonds relative to the Watson–Crick pair? and, second, how can such weak hydrogen bonds as in AF with a bond energy of −3.0 kcal/mol be important for accurate DNA replication?

To answer the first of these questions, we recall that the reduced bonding capabilities of F compared to T are sufficient to cause a sizeable elongation of the hydrogen bonds (*vide supra*). The longer hydrogen bonds in AF are therefore not necessarily caused by different steric shapes of F and T (i.e., different Pauli repulsion in A–F and A–T).[13(a)] Thus, we have explored the steric properties of F by compressing the AF hydrogen bonds N6–F4 and N1–C3 to the corresponding values 2.85 and 2.81 Å in the AT Watson–Crick geometry; we refer to this compressed complex as AF* (see Table I). Our quantitative analysis confirms that F is indeed a true isoster of T. This, follows from the fact that the steric repulsion, owing to ΔE_{Pauli}, is only 2.8 kcal/mol higher for AF* (41.6 kcal/mol) than for AT (38.7 kcal/mol).

The analysis of AF* also highlights the importance of hydrogen bonding in enzyme-catalyzed DNA replication. It has been convincingly shown[2,3(a)–3(s)] that this reaction involves a relatively tight active site, which requires the new base pair between template base and incoming base to conform to a geometry very close to the Watson–Crick geometry. If an incoming nucleotide is too large to fit into the active site of DNA polymerase, it causes steric repulsion and thus a high overall activation energy for the insertion of the nucleotide. This is schematically shown below in **1** (bold lines=active site; hatched area=spatial overlap of too large bases):

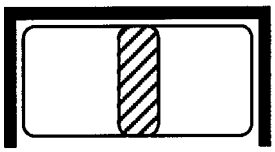

1

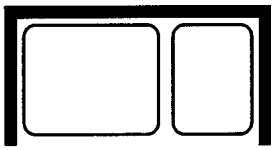

2

Base pairs of the right shape do fit into the active site without much repulsion (see **2** above). Such a situation is required for achieving a low overall activation barrier of the insertion. But the transition state is also stabilized by any favorable interaction that may occur between the bases. This is indicated by dots in **3** below:

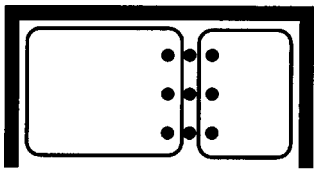

3

In case of the natural Watson–Crick pairs AT and GC, this favorable interaction is the hydrogen bond energies ΔE of

−13.0 and −26.1 kcal/mol, respectively.[12(b),14] We have shown previously that this intrinsic base-pairing interaction is affected neither by microsolvation of the major and minor grooves nor by the interaction between two stacked base pairs. Thus, the barrier for nucleotide insertion increases substantially if the stabilizing hydrogen bonds cannot be formed between the bases in the active site of the enzyme.

This is obvious for the relatively firmly bound natural Watson–Crick pairs AT and GC. But a similar argument holds true also for the weakly bound mimic AF. This is *not* obvious, at first sight, especially if one considers that the base pair in the geometrically confined active site of DNA polymerase, for which the compressed AF* complex is a model, is not even bound but instead slightly repulsive with a net hydrogen-bond interaction ΔE_{int} of ca 3 kcal/mol (Table I). Further analyses show, however, that without hydrogen bonding, the barrier for the process of nucleotide insertion would become much higher, in fact, restrictively high. This is clear if one realizes that the net interaction would increase much more strongly in AF* in the absence of the underlying electrostatic attraction (−22.6 kcal/mol) and covalent orbital interactions (−16.0 kcal/mol, Table I). The charge–transfer character of the latter is supported by the VDD charge decomposition analysis in Sec. III D. Loss of the orbital interactions ΔE_{oi}, for example, would upraise the overall barrier for the formation of a new base pair by 16.0 kcal/mol.

In practice, it is of course difficult to simply switch off the orbital interactions completely. They can be further reduced, however, if 2,4-difluorotoluene is replaced by a less polar mimic with even poorer electron donor and acceptor capabilities, for example, toluene (B). We find that the planar, C_S symmetric AB pair (Chart 2) is practically unbound at BP86/TZ2P. To simulate again a tight DNA-polymerase active site as proposed by Kool (*vide supra*),[2] we have compressed the AB pair to a geometry AB* in which the N6–H6···H4 and N1···H3–C3 hydrogen-bond distances adopt the values of the corresponding bonds in the equilibrium structure of AT (2.85 and 2.81 Å). And indeed, the net base-pairing interaction ΔE_{int} in AB* (9.2 kcal mol^{-1}) turns out substantially more repulsive than in AF* (2.9 kcal mol^{-1}). The reason is a significant decrease of both the orbital interactions ΔE_{oi} and electrostatic attraction ΔV_{elstat}, by a factor 2 (!) if compared to AT. Note that the steric repulsion term ΔE_{Pauli} does not vary so much along AT, AF*, and AB*.

Chart 2

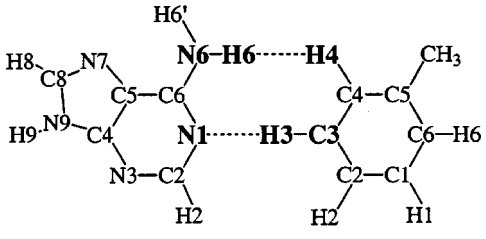

A B

The above results support aspects of both and lead to a synthesis of Kool's steric model of DNA replication[2] and the standard model that is based on hydrogen bonding.[1] They show that electrostatic and orbital interactions between DNA bases can contribute to reducing the overall barrier for insertion of a nucleotide if the net hydrogen bond strength is weak or even moderately repulsive. Note however that we have not computed the barrier height as such. Therefore, our results do not rule out the possibility of this barrier being low for other reasons, e.g., favorable solvent effects or stacking interactions.[3(n)–3(s)] It is conceivable that one or more of these factors are active in concert for achieving efficient and selective replication.

C. Extension of the VDD method for analyzing the charge distribution

The VDD method enables a decomposition of the deformation density associated with chemical bond formation between two molecular fragments into net changes per atom ΔQ_{A} and, furthermore, into the contributions from the σ and π electrons or, more generally, from the various irreducible representations Γ (see Sec. II C).[14] Our purpose here is to extend this functionality to also enable a decomposition of the charge redistribution per atom ΔQ_{A} into a component associated with the Pauli repulsion ΔE_{Pauli} and a component associated with the bonding orbital interactions ΔE_{oi},

$$\Delta Q_{\text{A}} = \Delta Q_{\text{A,Pauli}} + \Delta Q_{\text{A,oi}}. \tag{8}$$

This charge decomposition constitutes a complete bond analysis tool that mirrors all terms occurring in the bond energy decomposition of Eq. (2) described in Sec. II B (note that ΔV_{elstat} is not associated with any charge redistribution).

The Pauli repulsion ΔE_{Pauli} is the energy change associated with going from the superposition of unperturbed fragment densities $\rho_{\text{base1}} + \rho_{\text{base2}}$ to the wave function $\Psi^0_{\text{pair}} = \text{N}\,\hat{A}\,[\Psi_{\text{base1}}\Psi_{\text{base2}}]$ that properly obeys the Pauli principle through explicit antisymmetrization ($\hat{A}$ operator) and renormalization (N constant) of the product of fragment wave functions.[13(a)] The deformation density $\Delta\rho = \rho_{\text{pair}} - \rho_{\text{base1}} - \rho_{\text{base2}}$ associated with the formation of the overall molecule from its molecular fragments is now divided into two components [Eq. (9)],

$$\Delta\rho(\mathbf{r}) = \Delta\rho_{\text{Pauli}}(\mathbf{r}) + \Delta\rho_{\text{oi}}(\mathbf{r}). \tag{9}$$

Here, $\Delta\rho_{\text{Pauli}} = \rho^0_{\text{pair}} - \rho_{\text{base1}} - \rho_{\text{base2}}$ is associated with the Pauli repulsive orbital interactions and $\Delta\rho_{\text{oi}} = \rho_{\text{pair}} - \rho^0_{\text{pair}}$ with the bonding orbital interactions; ρ^0_{pair} is the density belonging to Ψ^0_{pair}.

Thus, the change in atomic charge caused by Pauli repulsion between the bases in the complex is defined by Eq. (10) and the corresponding change caused by charge transfer and polarization is given by Eq. (11),

$$\Delta Q_{\text{A,Pauli}} = -\int_{\substack{\text{Voronoi cell A}\\ \text{in pair}}} [\rho^0_{\text{pair}}(\mathbf{r}) - \rho_{\text{base1}}(\mathbf{r}) - \rho_{\text{base2}}(\mathbf{r})]\,d\mathbf{r}, \tag{10}$$

$$\Delta Q_{\text{A,oi}} = -\int_{\substack{\text{Voronoi cell A}\\ \text{in pair}}} [\rho_{\text{pair}}(\mathbf{r}) - \rho^0_{\text{pair}}(\mathbf{r})]\,d\mathbf{r}. \tag{11}$$

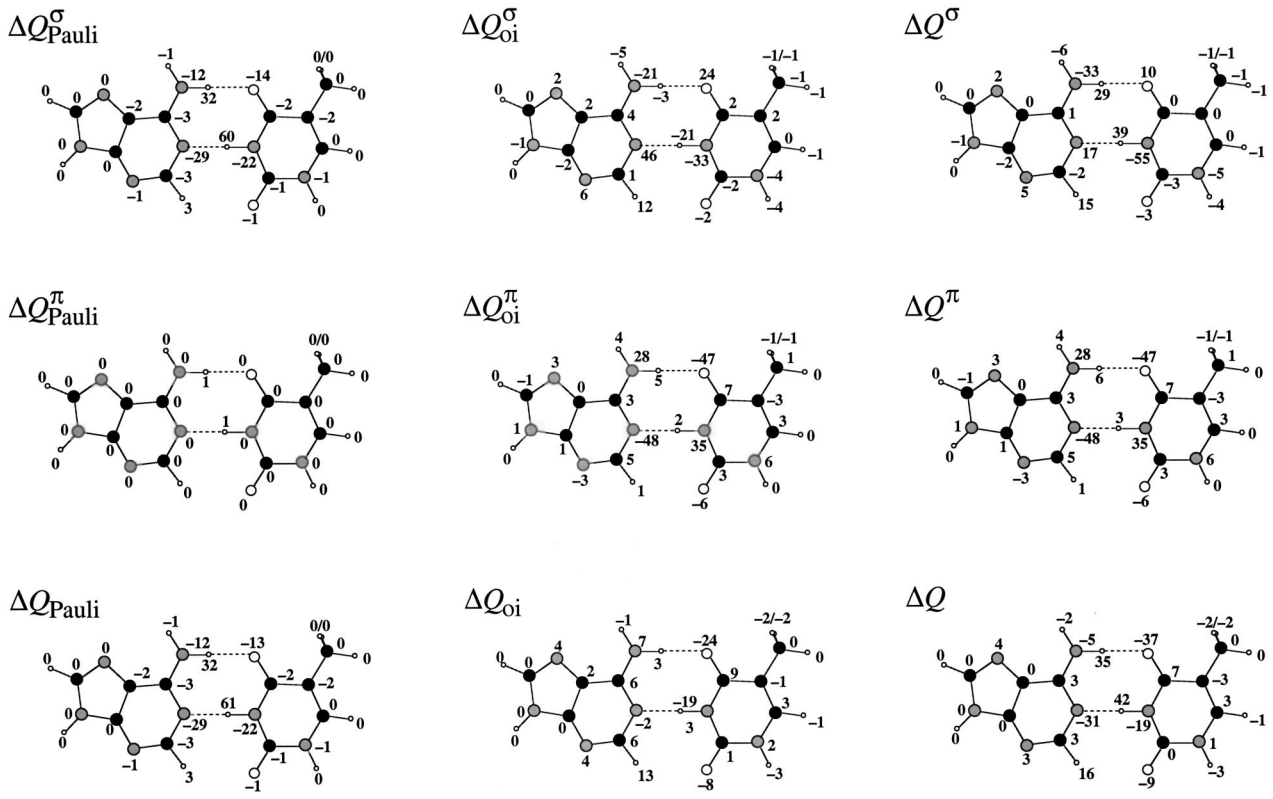

FIG. 6. Decomposition of VDD atomic charges (ΔQ, in milielectrons) associated with the formation of the AT pair form A and T into contributions from Pauli repulsion ($\Delta Q_{\mathrm{Pauli}}$) and bonding orbital interactions (ΔQ_{oi}) and into contributions stemming from the σ (ΔQ^{σ}) and π electrons (ΔQ^{π}) computed at BP86/TZ2P (see Chart 1 and Sec. III C).

With Eqs. (10) and (11), we are able to measure quantitatively and separately the charge redistributions associated with the energy component $\Delta E_{\mathrm{Pauli}}$ and with the orbital interaction component ΔE_{oi}.

The $\Delta Q_{\mathrm{A,Pauli}}$ and $\Delta Q_{\mathrm{A,oi}}$ can be further decomposed into contributions from the various irreducible representations Γ of the overall molecule, e.g., the σ and the π component (A' and A'' for the planar, C_s symmetric base pairs):

$$\Delta Q^{\Gamma}_{\mathrm{A,Pauli}} = -\int_{\substack{\text{Voronoi cell A}\\ \text{in pair}}} [\rho^{0,\Gamma}_{\mathrm{pair}}(\mathbf{r}) - \rho^{\Gamma}_{\mathrm{base1}}(\mathbf{r}) - \rho^{\Gamma}_{\mathrm{base2}}(\mathbf{r})]\, d\mathbf{r}, \tag{12}$$

$$\Delta Q^{\Gamma}_{\mathrm{A,oi}} = -\int_{\substack{\text{Voronoi cell A}\\ \text{in pair}}} [\rho^{\Gamma}_{\mathrm{pair}}(\mathbf{r}) - \rho^{0,\Gamma}_{\mathrm{pair}}(\mathbf{r})]\, d\mathbf{r}. \tag{13}$$

It appears that in particular the decomposition of $\Delta Q^{\sigma}_{\mathrm{A}}$ into a Pauli repulsion and a bonding orbital interaction component makes it possible to reveal small charge–transfer effects that are otherwise masked by the charge redistribution caused by Pauli repulsion (see Sec. III D).

D. Charge redistribution due to hydrogen bonding

The results of the VDD charge decomposition of the hydrogen bonds in AT, AF, and AF* are collected in Figs. 6–8. We first examine the more firmly bound AT complex for which we do indeed find the charge redistribution that is characteristic for donor–acceptor (or charge–transfer or covalent) interactions. This can be seen in Fig. 6 in the graphic labeled $\Delta Q^{\sigma}_{\mathrm{oi}}$ (first row, second graphic) which shows the changes in the atomic charges caused by the bonding orbital interactions in the σ-electron system [Eq. (14) with $\Gamma = \sigma$]: the electron–donor atoms of the N6–H6···O4 and N1···H3–N3 hydrogen bonds (see Chart 1) lose 24 and 46 milielectrons while the N–H bonds gain up to 54 milielectrons. This charge–transfer picture was found before by Fonseca Guerra *et al.*[14] but now, for the first time, we are able to separate the effect of Pauli repulsion between the lone pairs of the electron–donor atoms and the occupied N–H bonding orbitals ($\Delta Q^{\sigma}_{\mathrm{Pauli}}$ in Fig. 6) from the bonding donor–acceptor interactions ($\Delta Q^{\sigma}_{\mathrm{oi}}$ in Fig. 6). The effect of this Pauli repulsion is a depletion of charge density away from the central region of overlap and toward the periphery of the N6–H6···O4 and N1···H3–N3 hydrogen bonds. This causes a build-up of positive charge on the central hydrogen atom and of negative charge on the electronegative atoms at each side (see $\Delta Q^{\sigma}_{\mathrm{Pauli}}$ in Fig. 6). Note that this masks to some extent the effect of the charge–transfer interactions in the net changes in the atomic charges in the σ-electron system (ΔQ^{σ} in Fig. 6). Note also that in the overall change in atomic charges (ΔQ in Fig. 6), the charge–transfer effect of the hydrogen bonds is completely hidden by the charge redistribution in the π-electron system (ΔQ^{π} in Fig. 6). The latter polarizes in such a way that the build-up of positive or negative charges in the σ-electron system is cancelled or even overcompensated.

The charge redistribution is much less pronounced in AF

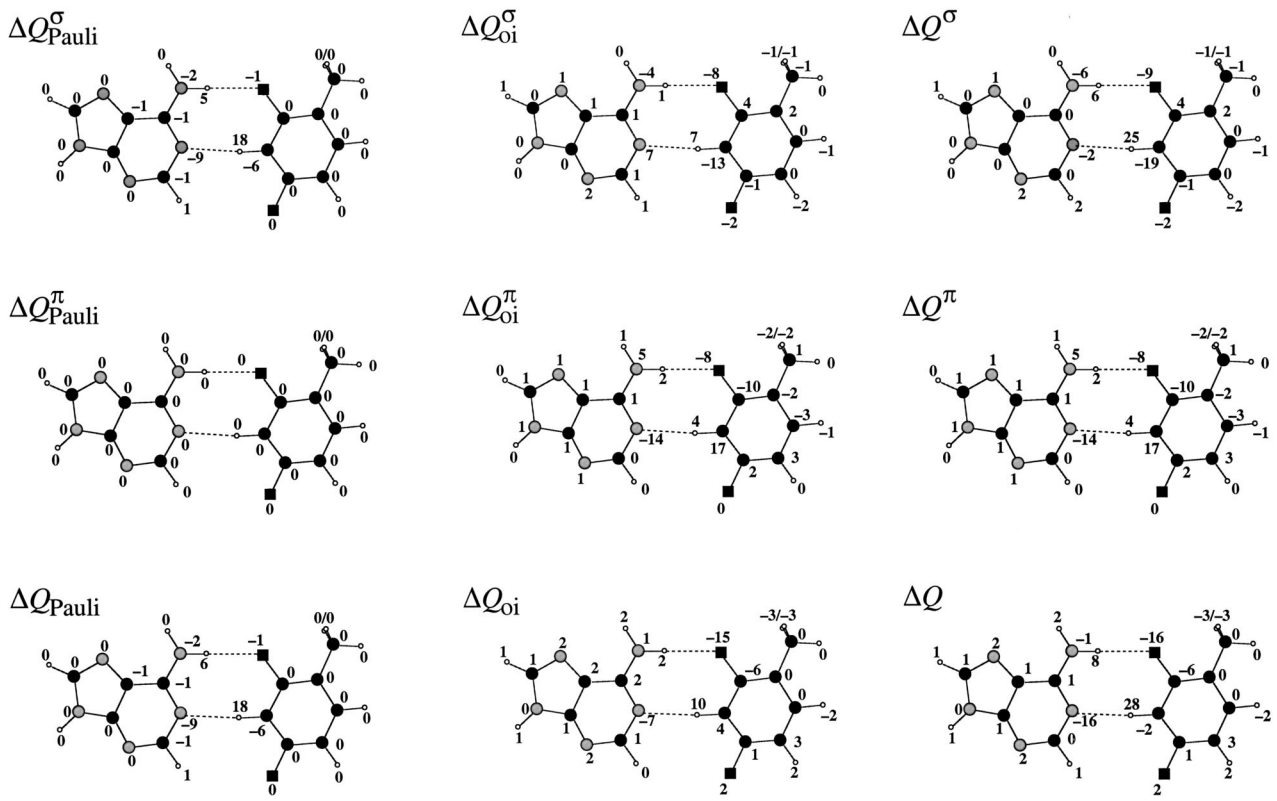

FIG. 7. Decomposition of VDD atomic charges (ΔQ, in milielectrons) associated with the formation of the AF pair form A and F into contributions from Pauli repulsion ($\Delta Q_{\mathrm{Pauli}}$) and bonding orbital interactions (ΔQ_{oi}) as well as into contributions stemming from the σ (ΔQ^{σ}) and π electrons (ΔQ^{π}) computed at BP86/TZ2P (see Chart 1 and Sec. III C).

than in AT (compare Figs. 7 and 6, respectively). This holds not only for the overall change in atomic charges (see ΔQ in Figs. 7 and 6) but also for the individual contributions (e.g., the bonding orbital interactions in the σ-electron system, see $\Delta Q^{\sigma}_{\mathrm{oi}}$ in Figs. 7 and 6). This finding is in line with AF being a significantly more weakly bound complex (compare Table I). The charge redistribution is significantly amplified, however, if the N6–H6···F4 and N1···H3–C3 hydrogen bonds in AF are compressed to the equilibrium distances of the corresponding bonds in the Watson–Crick pair AT, that is, going from AF to AF* (compare Figs. 7 and 8). For example, the build-up of charge on the atoms in the N1···H3–C3 hydrogen bond of AF* caused by the bonding orbital interactions in the σ-electron system amounts to +37, 0, and −30 milielectrons, respectively ($\Delta Q^{\sigma}_{\mathrm{oi}}$ in Fig. 8). These changes in the respective atomic charges reveal a significant increase of the charge–transfer interactions in the hydrogen bonds of AF* compared to that in AF. They already begin to approach the magnitude of the corresponding charge-transfer values of +46, −21, and −33 milielectrons in AT ($\Delta Q^{\sigma}_{\mathrm{oi}}$ in Fig. 6). This confirms, from a different perspective, the presence of the donor–acceptor orbital interactions in the hydrogen bonds between adenine and 2,4-difluorotoluene that assist in keeping the repulsion in the compressed AF* complex relatively low (see Sec. III B).

Finally, we point out a subtlety in the charge redistribution in AF and AF* (see Figs. 7 and 8). We discuss the effect for AF* in which the effect is most noticeable. The changes in atomic charges $\Delta Q^{\sigma}_{\mathrm{oi}}$ in N1···H3–C3 hydrogen bond in this complex show the loss of electronic charge density on the electron–donor atom N1 and gain of electronic charge density on the H3–C3 bond that is characteristic for donor–acceptor or charge–transfer interactions ($\Delta Q^{\sigma}_{\mathrm{oi}}$ in Fig. 8). Note however that the build-up of negative charge on the hydrogen atom is much smaller in AF* (Fig. 8, $\Delta Q^{\sigma}_{\mathrm{A,oi}}=0$ for H3) than in AT (Fig. 6, $\Delta Q^{\sigma}_{\mathrm{A,oi}}=-21$ milielectrons for H3). Even more striking is the situation for the N6–H6···F4 hydrogen bond for which the $\Delta Q^{\sigma}_{\mathrm{A,oi}}$ charges amount to −9, −2, and −3 milielectrons, that is, there is not the expected loss of charge from the F4 atom, which is supposed to donate charge out of its lone pair into the N6–H6 bond. An important source of this counterintuitive result is the more delocalized nature of the frontier orbitals on F compared to those on T discussed earlier, in Sec. III B (compare Figs. 4 and 5). The σ_{HOMO} of F, which acts as the lone pair on F4, also has a sizeable amplitude on H3 (Fig. 4). Thus, charge transfer from this orbital on F into the N6–H6 antibonding acceptor orbitals of A does not only cause the expected depletion of charge from F4 but also an *a priori* unexpected depletion of charge from H3. In addition, the H3–C3 antibonding $\sigma_{\mathrm{LUMO+1}}$ and $\sigma_{\mathrm{LUMO+3}}$ acceptor orbitals of F have also quite sizeable amplitudes on, amongst others, F4 (Fig. 4). As a consequence, charge transfer from the N1 lone pair of A into the H3–C3 acceptor orbitals of F leads not only to a build-up of negative charge on the H3–C3 bond but also to quite a sizeable one

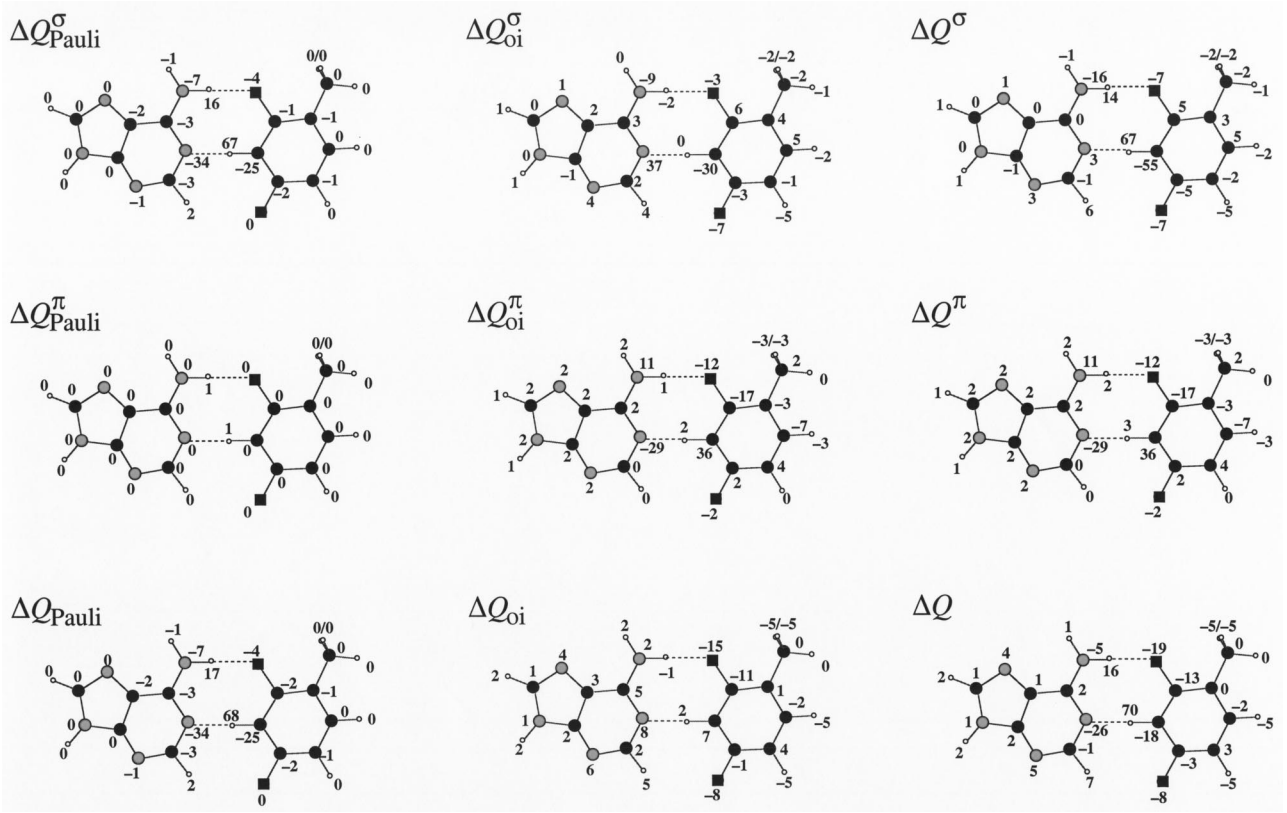

FIG. 8. Decomposition of VDD atomic charges (ΔQ, in milielectrons) associated with the formation of the AF* pair (AF pair compressed to AT Watson–Crick geometry) from A and F into contributions from Pauli repulsion ($\Delta Q_{\mathrm{Pauli}}$) and bonding orbital interactions (ΔQ_{oi}) as well as into contributions stemming from the σ (ΔQ^{σ}) and π electrons (ΔQ^{π}) computed at BP86/TZ2P (see Chart 1 and Sec. III C).

on F4. Overall, this causes the build-up of negative charge $\Delta Q^{\sigma}_{\mathrm{A,oi}}$ on H3 to be small (actually it is zero) while $\Delta Q^{\sigma}_{\mathrm{A,oi}}$ on F4 becomes negative instead of positive.

IV. CONCLUSIONS

Hydrogen bonding in AF, a weakly bound mimic of the Watson–Crick pair AT, is important for the experimentally observed ability of 2,4-difluorotoluene (F) to act as the complementary base of adenine (A) in enzyme-catalyzed DNA replication. This insight emerges from our theoretical study at BP86/TZ2P.

Although the hydrogen bonds in AF are relatively weak, they still possess an orbital interaction component that contributes not much less to the bonding forces than that of the stronger hydrogen bonds of AT: 36% vs 41%. In the steric model of DNA replication developed by Kool and co-workers,[2] the event of molecular recognition between DNA bases occurs as the complex between the template base and the incoming base fits into the sterically confined active site of DNA polymerase. This requires the new base pair to adopt the Watson–Crick geometry. Compressing the long hydrogen bonds in AF accordingly yields a structure AF*, which is only slightly repulsive. The orbital interactions in AF* are not much less bonding than in AT: -16 versus -22 kcal/mol. Thus, they are of crucial importance (together with the electrostatic attraction) for preventing the energy of this key structure in the replication mechanism to become restrictively high.

Our results reestablish hydrogen bonding as an essential factor in DNA replication involving natural bases as well as less polar mimics and they also confirm the importance of steric factors, in line with Kool's experimental work. In addition, they show that knowledge of the hydrogen bonding mechanism helps understanding the behavior of these bonds if they are deformed. Even if donor–acceptor orbital interactions are not visible at the ''surface'' of the net interaction (e.g., in AF*, which is located on a slightly repulsive point on the A–F potential energy surface) they can make an important contribution.

Of course, the reaction profile and overall barrier height of the complex multistep process of DNA replication also critically depend on many other factors, such as solvent effects, stacking interactions and the barrier of the $S_N2@P$ reaction that leads to the elongation of the backbone in the primer strand. However, isolating the effect of steric repulsion and hydrogen bonding also helps unraveling the role of these other factors. Eventually, this leads to a more detailed understanding of how the overall reaction profile arises. This will be the subject of forthcoming work.

ACKNOWLEDGMENTS

We thank the National Research School Combination–Catalysis (NRSC–C) for a postdoctoral fellowship for C.F.G. and the Netherlands Organization for Scientific Research (NWO) for financial support.

[1] (a) L. Stryer, *Biochemistry* (W. H. Freeman, New York, 1988); (b) A. Kornberg and T. A. Baker, *DNA Replication* (W. H. Freeman, New York, 1992).
[2] (a) K. M. Guckian, T. R. Krugh, and E. T. Kool, J. Am. Chem. Soc. **122**, 6841 (2000); (b) E. T. Kool, J. C. Morales, and K. M. Guckian, Angew. Chem. **112**, 1046 (2000); (c) J. C. Morales and E. T. Kool, J. Am. Chem. Soc. **122**, 1001 (2000); (d) K. M. Guckian, T. R. Krugh, and E. T. Kool, Nature Struct. Biol. **5**, 954 (1998); (e) J. C. Morales and E. T. Kool, *ibid.* **5**, 950 (1998); (f) D. Liu, S. Moran, and E. T. Kool, Chem. Biol. **4**, 919 (1997); (g) K. M. Guckian and E. T. Kool, Angew. Chem. **109**, 2942 (1997); (h) S. Moran, R. X.-F. Ren, S. Rumney IV, and E. T. Kool, J. Am. Chem. Soc. **119**, 2056 (1997); (i) B. A. Schweitzer, and E. T. Kool, *ibid.* **117**, 1863 (1995); (j) S. Moran, R. X.-F. Ren, and E. T. Kool, Proc. Natl. Acad. Sci. U.S.A. **94**, 10506 (1997); (k) E. T. Kool, Curr. Opin. Chem. Biol. **4**, 602 (2000); (l) L. Dzantiev, Y. O. Alekseyev, J. C. Morales, E. T. Kool, and L. J. Romano, Biochemistry **40**, 3215 (2001); (m) for an investigation on the proofreading of DNA, see J. C. Morales and E. T. Kool, *ibid.* **39**, 2626 (2000).
[3] (a) D. Summerer and A. Marx, Angew. Chem. **113**, 3806 (2001); Angew. Chem., Int. Ed. Engl. **40**, 3693 (2001); (b) M. Strerath, J. Cramer, T. Restle, and A. Marx, J. Am. Chem. Soc. **124**, 11230 (2002); (c) J. Cramer, M. Strerath, A. Marx, and T. Restle, J. Biol. Chem. **277**, 43593 (2002); (d) M. Strerath, D. Summerer, and A. Marx, ChemBioChem **6**, 578 (2002); (e) H. Echols and M. F. Goodman, Annu. Rev. Biochem. **60**, 477 (1991); (f) M. F. Goodman, Proc. Natl. Acad. Sci. U.S.A. **94**, 10493 (1997); (g) L. K. Clayton, M. F. Goodman, E. W. Branscomb, and D. J. Galas, J. Biol. Chem. **254**, 1902 (1979); (h) D. A. Lewis, K. Bebenek, W. A. Beard, S. H. Wilson, and T. A. Kunkel, *ibid.* **274**, 32924 (1999); (i) T. Matsuda, K. Bebenek, C. Masutani, F. Hanaoka, and T. A. Kunkel, Nature (London) **404**, 1011 (2000); (j) T. A. Kunkel and K. Bebenek, Annu. Rev. Biochem. **69**, 497 (2000); (k) K. A. Johnson, *ibid.* **62**, 685 (1993); (l) A. A. Johnson and K. A. Johnson, J. Biol. Chem. **276**, 38090 (2001); (m) J. D. Engel and P. H. Von Hippel, *ibid.* **253**, 935 (1978); (n) O. K. Abou-Zied, R. Jimenez, and F. E. Romesberg, J. Am. Chem. Soc. **123**, 4613 (2001); (o) Y. Wu, A. K. Ogawa, M. Berger, D. L. McMinn, P. G. Schultz, and F. E. Romesberg, *ibid.* **122**, 7621 (2000); (p) D. L. McMinn, A. K. Ogawa, Y. Wu, J. Liu, P. G. Schultz, and F. E. Romesberg, *ibid.* **121**, 11585 (1999); (q) M. Berger, A. K. Ogawa, D. L. McMinn, Y. Wu, P. G. Schultz, and F. E. Romesberg, Angew. Chem. **112**, 3069 (2000); Angew. Chem., Int. Ed. Engl. **39**, 2940 (2000); (r) A. K. Ogawa, Y. Wu, M. Berger, P. G. Schultz, and F. E. Romesberg, J. Am. Chem. Soc. **122**, 8803 (2000); (s) A. K. Ogawa, Y. Wu, D. L. McMinn, J. Liu, P. G. Schultz, and F. E. Romesberg, *ibid.* **122**, 3274 (2000); (t) C. L. Chepanoske, C. R. Langelier, N. H. Chmiel, and S. S. David, Org. Lett. **2**, 1341 (2000); (u) M. Ishikawa, I. Hirao, and S. Yokoyama, Tetrahedron Lett. **41**, 3931 (2000); (v) I. Hirao, T. Ohtsuki, T. Mitsui, and S. Yokoyama, J. Am. Chem. Soc. **122**, 6118 (2000); (w) H. Asanuma, T. Hishiya, T. Ban, S. Gotoh, and M. Komiyama, J. Chem. Soc., Perkin Trans. 2 **1998**, 1915 (1998).
[4] U. Diederichsen, Angew. Chem. **110**, 1745 (1998); Angew. Chem., Int. Ed. Engl. **37**, 1655 (1998).
[5] K. S. Schmidt, R. K. O. Sigel, D. V. Filippov, G. A. van der Marel, B. Lippert, and J. Reedijk, New J. Chem. **24**, 195 (2000).
[6] (a) D. Barsky, E. T. Kool, and M. E. Colvin, J. Biomol. Struct. Dyn. **16**, 1119 (1999); (b) B. D. Silverman, M. C. Pitman, and D. E. Platt, *ibid.* **16**, 1169 (1999); (c) F. Ryjácek, M. Kratochvíl, and P. Hobza, Chem. Phys. Lett. **313**, 393 (1999); (d) X. Wang and K. N. Houk, Chem. Commun. (Cambridge) **1999**, 2631 (1999); (e) C. Santhosh and P. C. Mishra, Int. J. Quantum Chem. **68**, 351 (1998); (f) T. A. Evans and K. R. Seddon, Chem. Commun. (Cambridge) **1997**, 2023 (1997); (g) M. Meyer and J. Sühnel, J. Biomol. Struct. Dyn. **15**, 619 (1997).
[7] (a) E. Cubero, C. A. Laughton, F. J. Luque, and M. Orozco, J. Am. Chem. Soc. **122**, 6891 (2000); (b) E. Cubero, E. C. Sherer, F. J. Luque, M. Orozco, and C. A. Laughton, *ibid.* **121**, 8653 (1999); (c) J. Florian, M. F. Goodman, and A. Warshel, J. Phys. Chem. B **122**, 10092 (2000).
[8] C. Fonseca Guerra and F. M. Bickelhaupt, Angew. Chem. **114**, 2194 (2002); Angew. Chem., Int. Ed. Engl. **41**, 2092 (2002).
[9] G. R. Desiraju and T. Steiner, *The Weak Hydrogen Bond* (Oxford University Press, Oxford, 1999).
[10] (a) V. R. Thalladi, H.-C. Weiss, D. Bläser, R. Boese, A. Nangia, and G. R. Desiraju, J. Am. Chem. Soc. **120**, 8702 (1998); (b) J. D. Dunitz and R. Taylor, Chem.-Eur. J. **3**, 89 (1997); (c) J. A. K. Howard, V. J. Hoy, D. O'Hagan, and G. T. Smith, Tetrahedron **52**, 12613 (1996).
[11] (a) T. Steiner, Chem. Commun. (Cambridge) **1997**, 727 (1997); (b) U. Koch and P. L. A. Popelier, J. Phys. Chem. **99**, 9747 (1995); (c) T. Steiner and W. Saenger, J. Am. Chem. Soc. **114**, 10146 (1992); (d) G. R. Desiraju, Acc. Chem. Res. **24**, 290 (1991); (e) R. Taylor and O. Kennard, J. Am. Chem. Soc. **104**, 5063 (1982); (f) M. Brandl, K. Lindauer, M. Meyer, and J. Sühnel, Theor. Chem. Acc. **101**, 101 (1999).
[12] (a) C. Fonseca Guerra, F. M. Bickelhaupt, J. G. Snijders, and E. J. Baerends, J. Am. Chem. Soc. **122**, 4117 (2000); (b) C. Fonseca Guerra and F. M. Bickelhaupt, Angew. Chem. **111**, 3120 (1999); Angew. Chem., Int. Ed. Engl. **38**, 2942 (1999); (c) C. Fonseca Guerra, F. M. Bickelhaupt, and E. J. Baerends, Crystal Growth Des. **2**, 239 (2002).
[13] (a) F. M. Bickelhaupt and E. J. Baerends, in *Reviews of Computational Chemistry*, edited by K. B. Lipkowitz and D. B. Boyd (Wiley-VCH, New York, 2000), Vol. 15, pp. 1–86; (b) R. Hoffmann, Angew. Chem. **94**, 725 (1982); Angew. Chem., Int. Ed. Engl. **21**, 711 (1982).
[14] C. Fonseca Guerra, F. M. Bickelhaupt, J. G. Snijders, and E. J. Baerends, Chem.-Eur. J. **5**, 3581 (1999).
[15] F. M. Bickelhaupt, N. J. R. van Eikema Hommes, C. Fonseca Guerra, and E. J. Baerends, Organometallics **15**, 2923 (1996).
[16] (a) G. te Velde, F. M. Bickelhaupt, S. J. A. van Gisbergen, C. Fonseca Guerra, E. J. Baerends, J. G. Snijders, and T. Ziegler, J. Comput. Chem. **22**, 931 (2001); (b) C. Fonseca Guerra, O. Visser, J. G. Snijders, G. te Velde, and E. J. Baerends, in *Methods and Techniques for Computational Chemistry*, edited by E. Clementi and G. Corongiu (STEF, Cagliari, 1995), pp. 305–395; (c) E. J. Baerends, D. E. Ellis, and P. Ros, Chem. Phys. **2**, 41 (1973); (d) E. J. Baerends and P. Ros, *ibid.* **8**, 412 (1975); (e) E. J. Baerends and P. Ros, Int. J. Quantum Chem., Symp. **12**, 169 (1978); (f) C. Fonseca Guerra, J. G. Snijders, G. te Velde, and E. J. Baerends, Theor. Chem. Acc. **99**, 391 (1998); (g) P. M. Boerrigter, G. te Velde, and E. J. Baerends, Int. J. Quantum Chem. **33**, 87 (1988); (h) G. te Velde and E. J. Baerends, J. Comput. Phys. **99**, 84 (1992); (i) J. G. Snijders, E. J. Baerends, and P. Vernooijs, At. Data Nucl. Data Tables **26**, 483 (1982); (j) J. Krijn and E. J. Baerends, *Fit-Functions in the HFS-Method; Internal Report (in Dutch)* (Vrije Universiteit, Amsterdam, 1984); (k) L. Versluis and T. Ziegler, J. Chem. Phys. **88**, 322 (1988); (l) J. C. Slater, *Quantum Theory of Molecules and Solids* (McGraw-Hill, New York, 1974), Vol. 4; (m) A. D. Becke, J. Chem. Phys. **84**, 4524 (1986); (n) A. Becke, Phys. Rev. A **38**, 3098 (1988); (o) S. H. Vosko, L. Wilk, and M. Nusair, Can. J. Phys. **58**, 1200 (1980); (p) J. P. Perdew, Phys. Rev. B **33**, 8822 (1986); *ibid.* **34**, 7406(E) (1986); (q) L. Fan and T. Ziegler, J. Chem. Phys. **94**, 6057 (1991).
[17] (a) K. Morokuma, J. Chem. Phys. **55**, 1236 (1971); (b) K. Kitaura and K. Morokuma, Int. J. Quantum Chem. **10**, 325 (1976); (c) T. Ziegler and A. Rauk, Inorg. Chem. **18**, 1755 (1979); (d) **18**, 1558 (1979); (e) Theor. Chim. Acta **46**, 1 (1977).
[18] (a) A. J. Stone, *The Theory of Intermolecular Forces* (Clarendon, Oxford, 1996); (b) A. J. Stone, Chem. Phys. Lett. **211**, 101 (1993).
[19] C. Kittel, *Introduction to Solid State Physics* (Wiley, New York, 1986).
[20] (a) G. A. Jeffrey, *An Introduction to Hydrogen Bonding* (Oxford University Press, New York, Oxford, 1997); (b) G. A. Jeffrey and W. Saenger, *Hydrogen Bonding in Biological Structures* (Springer-Verlag, Berlin, New York, Heidelberg, 1991).